Theory of the ordered phase in *A*-site antiferromagnetic spinels

SungBin Lee
Department of Physics, University of California–Santa Barbara, Santa Barbara, California 93106-9530, USA

Leon Balents
Kavli Institute for Theoretical Physics, University of California–Santa Barbara, Santa Barbara, California 93106-9530, USA

(Received 30 August 2008; published 22 October 2008)

Insulating spinel materials, with the chemical formula AB_2X_4, behave as diamond lattice antiferromagnets when only the *A*-site atom is magnetic. Many exhibit classic signatures of frustration, induced not geometrically but by competing first- and second-neighbor exchange interactions. In this paper, we further develop a theory [D. Bergman *et al.*, Nat. Phys. **3**, 487 (2007)] of the magnetism of these materials, focusing on the physics observable within the ordered state. We derive a phenomenological Landau theory that predicts the orientation of the spins within incommensurate spiral ordered states. It also describes how the spins reorient in a magnetic field and how they may undergo a low-temperature "lock-in" transition to a commensurate state. We discuss microscopic mechanisms for these magnetic-anisotropy effects. The reduction in the ordered moment by quantum fluctuations is shown to be enhanced due to frustration. Our results are compared to experiments on $MnSc_2S_4$, the best characterized of such *A*-site spinels, and more general implications are discussed. One prediction is that magnetically induced ferroelectricity is generic in these materials, and a detailed description of the relation of the electric polarization to the magnetism is given.

DOI: 10.1103/PhysRevB.78.144417 PACS number(s): 96.12.Hg, 75.30.Gw, 75.10.Hk, 75.30.Ds

I. INTRODUCTION

Frustrated magnets, in which competing exchange interactions cannot be simultaneously minimized, have long been a subject of theoretical and experimental study. Fundamental interest in them comes from their tendency to show more pronounced effects of fluctuations than their unfrustrated counterparts, and from prospects of observing exotic ground states as a consequence of frustration-induced sensitivity to weak perturbations. From a more practical materials science perspective, they are of particular recent interest because they tend to display noncollinear magnetic ordering. Such noncollinear ordering is quite generally connected to magnetically induced ferroelectricity,[1] making frustrated magnets a rich and productive hunting ground for multiferroics. In this paper, we study a particular class of frustrated spinel materials, with the chemical formula AB_2X_4, in which only the *A* atom is magnetic. Such materials are described as antiferromagnets on the diamond lattice. Somewhat surprisingly, although the diamond lattice is not *geometrically* frustrated and admits a simple two-sublattice collinear Néel state, many of these *A*-site magnetic spinels do exhibit significant signs of frustration. This includes a large ratio ("frustration parameter"[2]) $f=|\Theta_{CW}|/T_c$ between the Curie-Weiss temperature Θ_{CW} and an ordering or freezing temperature T_c. For example, experiments find $f\approx 10-20$ in $CoAl_2O_4$,[3,4] and $f\approx 12$ in $MnSc_2S_4$.[5] A recent theoretical study attributed this to the competition between first- and second-neighbor exchange interactions, J_1 and J_2, which can be comparable in these materials.[6] Theoretically, for $J_2/J_1>1/8$, the classical ground state becomes highly degenerate, consisting of coplanar spirals whose wave vector can be *arbitrarily* chosen on some "spiral surface" in momentum space. This degeneracy was suggested to be responsible for the observed signs of frustration, including large *f*, prominent diffuse neutron scattering in the paramagnetic state, and some low-temperature specific-heat anomalies. While encouraging, many of the predictions of this theory cannot currently be tested due to the absence of single-crystal neutron-scattering data.

In this paper, we develop this theory further, in order both to capture more detailed physical properties of this class of materials, and to make further predictions which might more readily be compared to existing and future experiments. We focus on physics rather than the results observed in the ordered state, which has been fairly well characterized in $MnSc_2S_4$. Specifically, we consider details of the *magnetic anisotropy* and the magnitude of the local ordered moments at low temperature. The theory of Ref. 6 was based on a Heisenberg model, which possesses O(3) [or SU(2)] spin-rotation symmetry and hence exhibits no preference for the absolute orientations of the spins themselves in the ordered state. Experimentally, in $MnSc_2S_4$ the spins are observed to lie on a definite plane. Moreover, the ordering wave vector describing the axis and pitch of the spiral in real space displays a "lock-in" behavior at low temperature, in which it becomes commensurate with the underlying spinel lattice. In the Heisenberg model, there is no explanation for this lock-in. We show here that both the choice of spiral plane and the commensurate lock-in of the spiral wave vector can be understood by considering magnetic-anisotropy effects. By an extended phenomenological Landau analysis, we can describe the magnetic orientation selection across the broader family of *A*-site spinels—which has not yet been studied experimentally—and predict some interesting "spin-flop" and reorientation effects in applied magnetic fields. We also consider, as mentioned, the value of the ordered moment, which experimentally shows a relatively large (for an $S=5/2$ spin) 20% suppression from the classical value. We show that, despite the large Mn^{2+} spins, this can actually be accounted for by quantum fluctuations provided further neighbor interactions are sufficiently small, due to the enhancement of fluctuations by frustration. Finally, we discuss

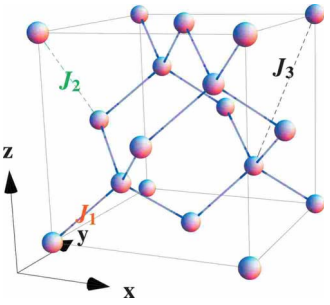

FIG. 1. (Color online) The diamond lattice with the first-, second-, and third-nearest-neighbor couplings J_1, J_2, and J_3, respectively.

the microscopic mechanisms behind the magnetic anisotropy of these materials, which may arise from both dipolar interactions and spin-orbit effects. In $MnSc_2S_4$, we find that spin-orbit-induced exchange anisotropy is the only one of these two mechanisms consistent with experimental observations.

We emphasize that though we pay particular attention to the comparison with $MnSc_2S_4$, the A-site spinels comprise a quite large set of interesting magnetic materials, and the theoretical analysis of this paper is formulated in such a way as to apply to the entire family. It therefore has numerous implications for many materials, and should be quite useful as a guide to future experiments. Of particular interest is the possibility of observing ferroelectricity and magnetoelectric effects in these compounds. Our modeling of magnetic anisotropy contains the essential ingredients for a theory of magnetically induced ferroelectricity. We present some basic observations of this type in Sec. VII, at the end of the paper.

The remainder of the paper is organized as follows. In Sec. II, we describe a phenomenological form of the magnetic anisotropy in terms of the order parameter, based on symmetry constraints, and the resulting ground states. In Sec. III, we discuss the magnetization process and a spin-flop transition in a field. Section IV discusses tendency of the spiral wave vector to lock to commensurate values and associated phase transitions. We show in Sec. V how quantum fluctuations can be included in the theory. Then, in Sec. VI we consider the possible microscopic sources of the magnetic anisotropy, and conclude that in $MnSc_2S_4$, it is most likely dominated by spin-orbit-induced exchange anisotropy. We conclude in Sec. VII with a summary of results and a discussion of experimental phenomena, including magnetically induced ferroelectricity. Some technical calculations are included in Appendixes A and C.

II. SPIRAL SPIN STATE AND SPIN-ROTATIONAL SYMMETRY BREAKING

A. Heisenberg model and its ground states

A minimal Heisenberg model description for the magnetism of these materials was studied in Ref. 6. Here the spins reside at the spinel A sites, which form a diamond lattice (see Fig. 1), composed of the two interpenetrating fcc lattices. The Hamiltonian, in zero magnetic field, is simply

$$H_{\mathrm{Heis}} = \frac{1}{2}\sum_{ij} J_{ij}\mathbf{S}_i \cdot \mathbf{S}_j. \tag{1}$$

Here we consider classical unit vector spins $|\mathbf{S}_i|=1$. We consider coupling between up to third-neighbor diamond sites, i.e., $J_{ij}=J_1,J_2,J_3$ for first-, second-, and third-neighbor sites, respectively. Though the diamond lattice with only nearest-neighbor spin exchange J_1 has an unfrustrated unique ground state, the inclusion of additional interactions (second-, third-nearest neighbor, etc.) rapidly produces frustration. Following the logic of Ref. 6, we presume that the first- and second-nearest-neighbor exchanges, J_1 and J_2, are dominant, and treat the third-neighbor coupling J_3 as a small (but important) degeneracy-breaking perturbation.

Ground states of this Hamiltonian can be found for arbitrary J_i by the method of Luttinger and Tisza. They take the form[6] of coplanar spirals

$$\mathbf{S}_i^{A(B)} = \frac{1}{2}\mathbf{d}e^{i\mathbf{k}\cdot\mathbf{x}_i \pm i\gamma/2} + \mathrm{c.c.}, \tag{2}$$

where the order parameter $\mathbf{d}$ is a complex three-component vector satisfying

$$\mathbf{d}\cdot\mathbf{d} = 0,$$

$$\mathbf{d}\cdot\mathbf{d}^* = 2. \tag{3}$$

These two constraints, as well as the choice of γ, ensure that the magnitude of each spin is unity, $|\mathbf{S}_i|=1$. One has

$$\gamma = \arg\left[\sum_{i\in A, j\in B}{}' J_{ij}e^{i\mathbf{k}\cdot\mathbf{r}_{ij}}\right], \tag{4}$$

where the sum Σ' is taken over sites is taken over all sites j on the B sublattice, with i fixed as an arbitrary A sublattice site. The physical meaning of $\mathbf{d}$ is made clear by solving the constraint

$$\mathbf{d} = \hat{\mathbf{e}}_1 + i\hat{\mathbf{e}}_2 \tag{5}$$

and defining

$$\hat{\mathbf{e}}_3 = \hat{\mathbf{e}}_1 \times \hat{\mathbf{e}}_2 = \frac{i}{2}\mathbf{d}\times\mathbf{d}^*. \tag{6}$$

Here $\hat{\mathbf{e}}_1$, $\hat{\mathbf{e}}_2$, and $\hat{\mathbf{e}}_3$ are three mutually orthogonal unit vectors. The first two span the plane on which the spins reside, and $\hat{\mathbf{e}}_3$ is the unique normal to the plane. A phase rotation of $\mathbf{d}$ rotates the spins within the plane, or equivalently translates the spiral along its axis while leaving the spin plane and hence $\hat{\mathbf{e}}_3$ unchanged.

The energy of spiral states of this type is readily evaluated. It is sufficient to linearize in J_3, in which case one finds the energy per unit cell (this is twice the energy per spin),

$$E_J(\mathbf{k}) = E_{12}(\mathbf{k}) + E_3(\mathbf{k}), \tag{7}$$

where E_{12} and E_3 are the contributions from the large J_1 and J_2 exchanges and the smaller J_3 exchange, respectively. Explicitly,

$$E_{12} = 16J_2\left(\Lambda(\mathbf{k}) - \frac{|J_1|}{8J_2}\right)^2 - 4J_2 - \frac{J_1^2}{4J_2}, \tag{8}$$

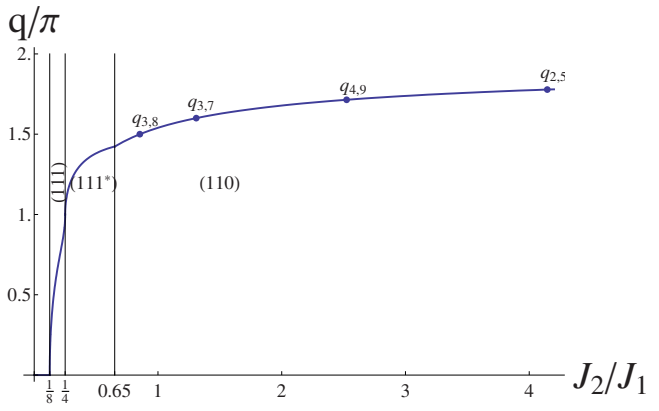

FIG. 2. (Color online) The selected wave vector of the diamond antiferromagnet for antiferromagnetic J_3. We plot q/π as a function of J_2/J_1, where the ground-state wave vector has the form (q,q,k). The direction (choice of k) is indicated by the labels (111), (111*), and (110)—see text and Appendix A for details—in each of the regions separated by vertical lines. The first four lowest-order commensurate wave vectors $q_{m,n}$ for which lock-in transitions are expected are also indicated by labeled dots (see Sec. IV).

$$\delta E_3 = J_3 \frac{\Sigma(\mathbf{k})}{\Lambda(\mathbf{k})}, \tag{9}$$

with

$$\Lambda(\mathbf{k}) = \left[\cos^2\frac{k_x}{4}\cos^2\frac{k_y}{4}\cos^2\frac{k_z}{4} + \sin^2\frac{k_x}{4}\sin^2\frac{k_y}{4}\sin^2\frac{k_z}{4} \right]^{1/2},$$

$$\Sigma(\mathbf{k}) = \cos k_x \left(1 + 2\cos\frac{k_y}{2}\cos\frac{k_z}{2} \right) + 2\cos\frac{k_x}{2}\cos\frac{k_y}{2} + \text{cyclic perms.} \tag{10}$$

Treating J_3 perturbatively, we first minimize E_{12}. For $J_2/|J_1| < 1/8$, the minimum occurs for $\mathbf{k}=0$, while for $J_2/|J_1| > 1/8$, it occurs along the surface defined by $\Lambda(\mathbf{k}) = |J_1|/8J_2$. In the latter case, the third-nearest-neighbor exchange breaks the "spiral-surface" degeneracy. A combination of analytical and numerical arguments (see Appendix A) determines the selected wave vectors on the spiral surface. We assume antiferromagnetic $J_3 > 0$, in which case the minimum energy is realized with a wave vector of the form $\mathbf{q} = (q,q,k)$, where the relation of k to q varies depending upon the magnitude of J_2/J_1. The direction of the wave vector thereby varies from the (111) to the (110) directions, with an intermediate (111*) region in which the k is chosen as close as possible to q since the (111) directions do not intersect the spiral surface. See Fig. 2 and Appendix A for further details. We note that this wave vector, determined from the third-nearest-neighbor exchange J_3, is different from the one determined by thermal fluctuations.[6]

For the specific material $MnSc_2S_4$, the magnetic structure is known from neutron diffraction.[7] At low temperature the ordering wave vector is $\mathbf{k}=\mathbf{q} \equiv 3\pi/2(1,1,0)$, and the refinement indicates ferromagnetic $J_1 < 0$. Comparison to the theoretical structure and the measured Curie-Weiss temperature allows one to constraint the couplings.[6] When J_3 is very small, one has $J_1 \simeq -10.5K$ and $J_2 \simeq 8.75K$. More generally, fixing $\mathbf{k}=3\pi/2(1,1,0)$, one has

$$J_3/|J_1| = \frac{-1 + (4 - 2\sqrt{2})J_2/|J_1|}{4\sqrt{2} - 3}. \tag{11}$$

From this relation, $J_2/|J_1|$ varies from 0.88 to 0.94 when $J_3/|J_1|$ is increased from 0.01 to 0.04.

B. Magnetic anisotropy

The Heisenberg model leaves the plane and phase of the spin spiral undetermined because they can be continuously rotated using the SU(2) symmetry of the Hamiltonian. In reality, this symmetry is broken by the crystal lattice and "spin-orbit" effects (in fact arising from both quantum-mechanical spin-orbit coupling and dipolar interactions between spins) that couple spin and spatial rotations. Indeed, in $MnSc_2S_4$, it is known that the spins in the (110) spiral lie on a (001) plane. This is determined by physics outside the Heisenberg model. Furthermore, the commensurate *magnitude* of the wave vector—$\mathbf{q}=q_0(1,1,0)$ with $q_0=3\pi/2$ *exactly* within experimental resolution—is also related to anisotropy effects. In the Heisenberg model, obtaining this value of q_0 at $T=0$ requires fine-tuning of the ratio of J_2/J_1, and even with such tuning, the magnitude would generally deviate at $T>0$.

To understand these effects, we first adopt a phenomenological Landau theoretic approach constrained only by symmetry. This consists of time-reversal invariance, which reverses spins, and the space group $Fd\bar{3}m$ of the spinel lattice. The full space group is generated by six operations, which may be expressed in terms of translations $\mathcal{T}_\mathbf{t}$ by the vector $\mathbf{t}$, rotations $\mathcal{R}_\mathbf{n}[\theta]$ by angle θ about the $\mathbf{n}$ axis, and the inversion $\mathcal{I}$ about the origin. In our coordinate system, the generators $\mathcal{G}_i$ are

$$\mathcal{G}_1 = \mathcal{T}_{3/4,1/4,1/2} \circ \mathcal{R}_{001}[\pi], \tag{12}$$

$$\mathcal{G}_2 = \mathcal{T}_{1/4,1/2,3/4} \circ \mathcal{R}_{010}[\pi], \tag{13}$$

$$\mathcal{G}_3 = \mathcal{R}_{111}\left[\frac{2\pi}{3}\right], \tag{14}$$

$$\mathcal{G}_4 = \mathcal{T}_{3/4,1/4,1/2} \circ \mathcal{R}_{110}[\pi], \tag{15}$$

$$\mathcal{G}_5 = \mathcal{I}, \tag{16}$$

$$\mathcal{G}_6 = \mathcal{T}_{0,1/2,1/2}. \tag{17}$$

Because the spin is a pseudovector, its transformation under each of these operations is given by

$$\mathbf{S}(\mathbf{x}) \to \mathrm{Det}[\hat{\mathbf{O}}] \cdot \hat{\mathbf{O}}^{-1} \cdot \mathbf{S}(\hat{\mathbf{O}} \cdot \mathbf{r} + \mathbf{t}), \tag{18}$$

where $\hat{\mathbf{O}}$ is the orthogonal matrix giving the rotation or inversion part of the operation $(\mathbf{r} \to \hat{\mathbf{O}} \cdot \mathbf{r})$ and $\mathbf{t}$ is the translation vector.

We are interested in the effect of spin-orbit coupling

within the ordered phase of these materials. In this case, the symmetry is already reduced from that of the full crystal by the magnetic order. Specifically, we assume an ordered state of the form predicted by the Heisenberg model, i.e., satisfying Eq. (2) with $\mathbf{k}$ determined to be one of the values selected by J_1, J_2, and J_3 but with $\mathbf{d}$ arbitrary up to the constraints in Eq. (3). We seek a Landau free energy as a function of $\mathbf{d}$. Since we restrict to a fixed $\mathbf{k}$, we should consider only those symmetry operations which leave $\mathbf{k}$ invariant (up to inversion). This is the *little group* of the wave vector $\mathbf{k}$. Under each element in this little group, because the wave vector is invariant, one can define a corresponding transformation for $\mathbf{d}$, under which the free energy must be invariant.

We consider the two major regimes of phase space in which the form of $\mathbf{k}$ is simple. For $1/8 < J_2/|J_1| < 1/4$, we have $\mathbf{k}=k(1,1,1)$. The little group is generated by the transformations $\mathcal{G}_3$, $\mathcal{G}_5$, and $\mathcal{G}_6$ in this case. Under these operations, the order parameter transforms according to

$$\mathcal{G}_3:\ d_1 \to d_3, \quad d_2 \to d_1, \quad d_3 \to d_2,$$

$$\mathcal{G}_5:\ \mathbf{d} \to \mathbf{d}^*,$$

$$\mathcal{G}_6:\ \mathbf{d} \to e^{ik}\mathbf{d}. \tag{19}$$

In the case $J_2/J_1 \gtrsim 0.7$, one has $\mathbf{k}=k(1,1,0)$, for which the little group is generated instead by $\mathcal{G}_1$, $\mathcal{G}_4$, $\mathcal{G}_5$, and $\mathcal{G}_6$. Under these operations, we find

$$\mathcal{G}_1:\ \mathbf{d} \to e^{-ik}\mathbf{d}^*,$$

$$\mathcal{G}_4:\ \mathbf{d} \to e^{ik}\begin{pmatrix} 0 & 1 & 0 \\ 1 & 0 & 0 \\ 0 & 0 & 1 \end{pmatrix}\mathbf{d},$$

$$\mathcal{G}_5:\ \mathbf{d} \to \mathbf{d}^*,$$

$$\mathcal{G}_6:\ \mathbf{d} \to e^{ik/2}\mathbf{d}. \tag{20}$$

Using these symmetries, we can determine the most general allowed form of the free energy at any given order in $\mathbf{d}$, for each of these two cases. Our focus is on terms which violate SU(2) symmetry, induced by spin-orbit coupling or dipolar interactions. As usual within Landau theory, we expect terms which involve smaller powers of the order parameter to be the most important. We therefore consider the leading *quadratic* terms other than the trivial $|\mathbf{d}|^2$ one. For the $\mathbf{k}=(k,k,k)$ states, we find a single nontrivial invariant:

$$f_{111}(\mathbf{d}) \equiv c[d_3^*(d_1+d_2)+d_2^*(d_1^*+d_3)+d_1^*(d_2+d_3)]. \tag{21}$$

For the wave vector $k(1,1,0)$, the quadratic free energy contains two nontrivial invariants:

$$f_{110}(\mathbf{d}) \equiv c_1(d_1^* d_2 + \text{c.c.}) + c_2 d_3^* d_3. \tag{22}$$

These quadratic terms distinguish different planes in which the spins spiral energetically. We note that both f_{111} and f_{110} are invariant under arbitrary phase rotations of the $\mathbf{d}$ fields. Physically, this implies that rotations of the vectors $\hat{\mathbf{e}}_1$ and $\hat{\mathbf{e}}_2$ within the plane normal to $\hat{\mathbf{e}}_3$ cost no energy. Therefore we expect that these terms may be rewritten in terms of $\hat{\mathbf{e}}_3$ alone. This is indeed the case. To do so, it is convenient to introduce a parametrization of $\mathbf{d}$ which solves the constraints in Eq. (3):

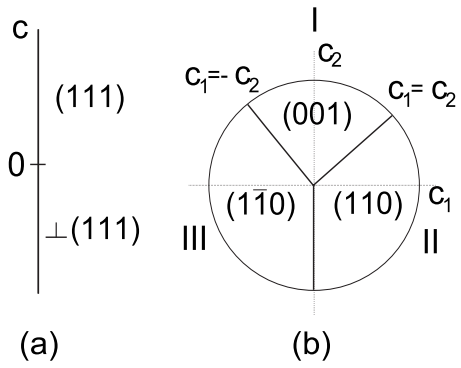

FIG. 3. Directions of the normal $\hat{\mathbf{e}}_3$ to the plane of spin ordering selected by magnetic-anisotropy terms in the cases (a) of a (111) wave vector and (b) of a (110) wave vector. In (a), the symbol $\perp(111)$ indicates that any plane with $\hat{\mathbf{e}}_3 \cdot (111)=0$ is a ground state.

$$\mathbf{d} = z_\alpha \boldsymbol{\epsilon}_{\alpha\beta}\boldsymbol{\sigma}_{\beta\gamma}z_\gamma, \tag{23}$$

where we have defined the spinor z_α,

$$z = (e^{i\phi_1}\cos\theta, e^{i\phi_2}\sin\theta), \tag{24}$$

which satisfies $|z_1|^2+|z_2|^2=1$. Here $\boldsymbol{\sigma}$ is the vector of Pauli matrices, and $\boldsymbol{\epsilon}_{\alpha\beta}$ is the antisymmetric matrix with $\boldsymbol{\epsilon}_{12}=1$. It is straightforward to show that

$$\hat{\mathbf{e}}_3 = z_\alpha^* \boldsymbol{\sigma}_{\alpha\beta} z_\beta. \tag{25}$$

By explicit evaluation using Eqs. (23) and (24), one can readily show

$$f_{111} = c(1-[e_3^x+e_3^y+e_3^z]^2), \tag{26}$$

$$f_{110} = -2c_1 e_3^x e_3^y + c_2[(e_3^x)^2+(e_3^y)^2]. \tag{27}$$

Now the energetically preferred plane for the spins is apparent. They are illustrated in Fig. 3. For $\mathbf{k}=(k,k,k)$, the ground state has $\hat{\mathbf{e}}_3=(1,1,1)/\sqrt{3}$ for $c>0$, and $\hat{\mathbf{e}}_3\cdot(1,1,1)=0$ for $c<0$ (i.e., in the latter case, the vector $\hat{\mathbf{e}}_3$ is still free to rotate anywhere within a plane). For $\mathbf{k}=(k,k,0)$, three distinct directions of $\hat{\mathbf{e}}_3$ are possible depending upon the values of c_1 and c_2—see Fig. 3 for details.

At this stage it is possible to compare with experimental results on $MnSc_2S_4$. Refined neutron-scattering data in Ref. 7 indicated spiral order of the type discussed here with wave vector $\mathbf{q}=(q,q,0)$ and spins aligned within the (001) plane. We see that the Landau theory indeed captures this order provided the phenomenological parameters c_1 and c_2 are taken to lie within region I of the phase diagram in Fig. 3. Note that this is not "fine-tuning," as this region occupies a finite fraction of the phase diagram. However, it is still inter-

esting to understand the microscopic reason for the system to be in region I rather than region II or III. We will return to this question in Sec. VI.

III. MAGNETIZATION PROCESS

In this section, we consider the evolution of the spin state in an applied magnetic field. Neglecting magnetic anisotropy, we may expect a smooth evolution, in which the spins adopt a canted (conical) configuration with a nonvanishing component along the field, and this canting gradually increases until the spins become fully aligned at saturation. In the presence of magnetic anisotropy, however, the spins have an intrinsic preference for particular planes, which, in some field orientations, competes with the tendency of the spins to adapt to the field. We study these two situations below.

A. Heisenberg model

We first neglect magnetic anisotropy and consider simply the classical Heisenberg Hamiltonian with an added Zeeman magnetic field,

$$H_{J,h} = \frac{1}{2}\sum_{i,j} J_{ij}\mathbf{S}_i \cdot \mathbf{S}_j - \sum_i \mathbf{h}\cdot\mathbf{S}_i. \tag{28}$$

We seek ground states with normalized spins $|\mathbf{S}_i|=1$, using following ansatz:

$$\mathbf{S}_i^{A(B)} = \frac{1}{2}\mathbf{d}e^{i(\mathbf{k}\cdot\mathbf{x}_i \pm \gamma/2)} + \text{c.c.} + \mathbf{m}, \tag{29}$$

with the constraints

$$\mathbf{d}\cdot\mathbf{d} = 0, \tag{30}$$

$$\mathbf{d}\cdot\mathbf{m} = 0, \tag{31}$$

$$\frac{1}{2}\mathbf{d}\cdot\mathbf{d}^* + \mathbf{m}^2 = 1. \tag{32}$$

We now evaluate the energy for these states. It is necessary to consider ferromagnetic and antiferromagnetic J_1 separately.

1. Ferromagnetic J_1

In the ferromagnetic case, evaluating the energy per unit cell using the Hamiltonian in Eq. (28), one obtains

$$E_{J,h}^{\text{FM}} = \frac{1}{2}E_J(\mathbf{k})|\mathbf{d}|^2 + |\mathbf{m}|^2 E_J(0) - 2\mathbf{h}\cdot\mathbf{m}. \tag{33}$$

Here $E_J(\mathbf{k})$ is the energy function for a pure spiral in zero field, given in Eq. (7).

This energy function is minimized as follows. Only the third term is dependent upon the orientation of $\mathbf{d}$ and $\mathbf{m}$, and it is minimized if we choose $\mathbf{m}=m\hat{\mathbf{h}}$ along the field direction. Then we must choose, as similarly done in Eq. (5),

$$\mathbf{d} = \sqrt{1-m^2}(\hat{\mathbf{e}}_1 + i\hat{\mathbf{e}}_2), \tag{34}$$

with $\hat{\mathbf{e}}_3=\hat{\mathbf{e}}_1\times\hat{\mathbf{e}}_2=\hat{\mathbf{h}}$. This indeed describes a conical spin state. For fixed m and hence $|\mathbf{d}|^2=2(1-m^2)$, the energy is minimized by the wave vector $\mathbf{k}=\mathbf{q}$ which minimized $E_J(\mathbf{k})$. This implies that the wave vector is independent of magnetic field. Finally, we can minimize over m, which gives

$$m = \frac{h}{h_{\text{sat}}}, \tag{35}$$

which is valid for fields below the saturation field, which in this ferromagnetic case is

$$h_{\text{sat}}^{\text{FM}} = E_J(0) - E_J(\mathbf{q}) \equiv \Delta E. \tag{36}$$

Here we define ΔE for later convenience. We see that the magnetization increases perfectly and linearly up to saturation. The saturation field itself varies with the exchange couplings and in particular J_2/J_1 in a nontrivial manner as the ordering wave vector $\mathbf{q}$ varies—see Fig. 4. Since the ground state itself is ferromagnetic for $J_2<J_1/8$, the saturation field vanishes in this region.

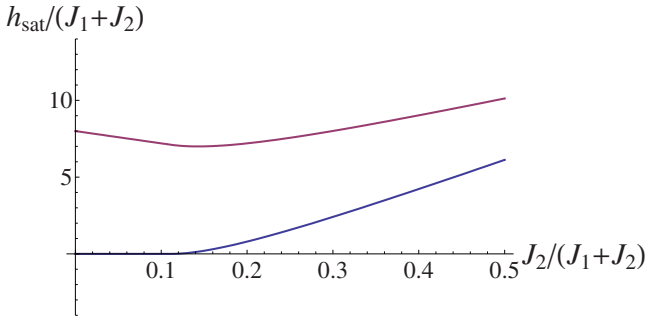

FIG. 4. (Color online) Saturation fields $h_{\text{sat}}/(J_1+J_2)$ as a function of $J_2/(J_1+J_2)$, for the ferromagnetic (lower curve) and antiferromagnetic (upper curve) cases.

2. Antiferromagnetic J_1

Next consider the case of antiferromagnetic J_1. In this case, the energy function is

$$E_{J,h}^{\text{AFM}} = \frac{1}{2}E_J(\mathbf{k})|\mathbf{d}|^2 + [E_J(0) + 8J_1]|\mathbf{m}|^2 - 2\mathbf{h}\cdot\mathbf{m}. \tag{37}$$

The difference from Eq. (33) can be understood as arising because of the cost $8J_1$ of flipping the four nearest-neighbor bonds per site from antiparallel to parallel spin alignment. Repeating the analysis in Sec. III A 1, we again find a linear magnetization curve [i.e., Eq. (35)], but with the saturation field

$$h_{\text{sat}}^{\text{AFM}} = 8J_1 + \Delta E. \tag{38}$$

B. Anisotropy and spin-flop transition

We now turn to the effects of magnetic anisotropy and in particular the competition between the magnetic field and the intrinsic preference for the spin-ordering plane. Lacking a microscopic model for the anisotropy, we cannot reliably explore the full phase diagram for all fields. However, since we expect that the anisotropy is relatively weak compared to the exchange, the portion of phase space in which the field and

anisotropy are actually competitive is restricted to small fields. In this regime, the contribution of the anisotropy to the energy should be approximately unchanged from that at zero field. Hence we may model it by the *same* phenomenological function given in Sec. II B. That is, we add to the Heisenberg energy $E_{J,h}$ the terms f_{111} and f_{110}, as appropriate.

Let us focus on ferromagnetic J_1 with $\mathbf{q}=(q,q,0)$ for simplicity. The discussion is not significantly modified in the antiferromagnetic case. The energy function is now

$$E_{\text{tot}}^{\text{FM}} = \frac{1}{2}E_J(\mathbf{k})|\mathbf{d}|^2 + |\mathbf{m}|^2 E_J(0) - 2\mathbf{h}\cdot\mathbf{m} + f_{110}[\mathbf{d}]. \quad (39)$$

In small fields, we may fix $\mathbf{k}=\mathbf{q}$ the zero-field ordering wave vector which minimized E_J. We can use Eq. (34), with however $\hat{\mathbf{e}}_3=\hat{\mathbf{m}}$ not necessarily parallel to $\mathbf{h}$. Inserting this into the energy, we find

$$E_{\text{tot}}^{\text{FM}} = E_J(\mathbf{q}) + \Delta E|\mathbf{m}|^2 - 2\mathbf{h}\cdot\mathbf{m} + f_{110}[\hat{\mathbf{e}}_3 = \hat{\mathbf{m}}], \quad (40)$$

where $f_{110}[\hat{\mathbf{e}}_3]$ is given in Eq. (27). Here we have approximated $m\approx 0$ in the anisotropy term, since the neglected corrections are of $O(m^2 c_{1,2})$, i.e., small in both the magnetization and the anisotropy.

We can now minimize Eq. (40) over the magnitude of the magnetization at fixed orientation, which gives

$$m = \frac{\mathbf{h}\cdot\hat{\mathbf{m}}}{\Delta E}, \quad (41)$$

and the energy, which now depends only upon the orientation $\hat{\mathbf{m}}$,

$$E_{\text{tot}}^{\text{FM}}(\hat{\mathbf{m}}) = -\frac{(\mathbf{h}\cdot\hat{\mathbf{m}})^2}{\Delta E} + f_{110}[\hat{\mathbf{m}}] \quad (42)$$

up to constants independent of $\hat{\mathbf{m}}$. We caution that in these expressions, it is possible to take $\hat{\mathbf{m}}\cdot\mathbf{h}=0$, in which case the actual magnetization vanishes, but $\hat{\mathbf{m}}=\hat{\mathbf{e}}_3$ still defines the plane of the spiral.

To determine $\hat{\mathbf{m}}$, we must minimize Eq. (42). Let us first consider the special case $c_1=0$, $c_2>0$. Then we may presume that $\hat{\mathbf{m}}$ lies on the plane spanned by $\hat{\mathbf{z}}$ and $\hat{\mathbf{h}}$. Taking the angle of $\hat{\mathbf{m}}$ with the z axis as θ and the angle of $\hat{\mathbf{h}}$ with the z axis as θ_h, the energy is

$$E_{\text{tot}}^{\text{FM}} = -c_2\cos^2\theta - \frac{h^2}{\Delta E}\cos^2(\theta-\theta_h), \quad (43)$$

$$= -A\cos[2(\theta-\theta_0)] + \text{const}, \quad (44)$$

where

$$A = \frac{c_2}{4}\sqrt{1+4\mathbf{h}^2+4\mathbf{h}\cos 2\theta_h}, \quad (45)$$

$$\theta_0 = \frac{1}{2}\text{acos}\left[\frac{1+2\mathbf{h}^2\cos 2\theta_h}{\sqrt{1+4\mathbf{h}^4+4\mathbf{h}^2\cos 2\theta_h}}\right], \quad (46)$$

with $\mathbf{h}=h/\sqrt{c_2\Delta E}$. The angle θ_0 obviously gives the orientation of $\hat{\mathbf{m}}$. Interestingly, it is an analytic function of h *except* at $\theta_h=\pi/2$, i.e., when the magnetic field is perpendicular to the (100) axis. As this value of θ_h is approached, $\theta_0(\mathbf{h})$ becomes sharper and approaches a step function: $\theta_0(\mathbf{h};\theta_h=\pi/2)=\frac{\pi}{2}\Theta(\mathbf{h}-1/\sqrt{2})$. It is also instructive to plot the magnitude of the magnetization, $m(\mathbf{h})$. The magnetization jumps at $\mathbf{h}=1/\sqrt{2}$ for $\theta_h=\pi/2$ but is otherwise continuous (see Fig. 5).

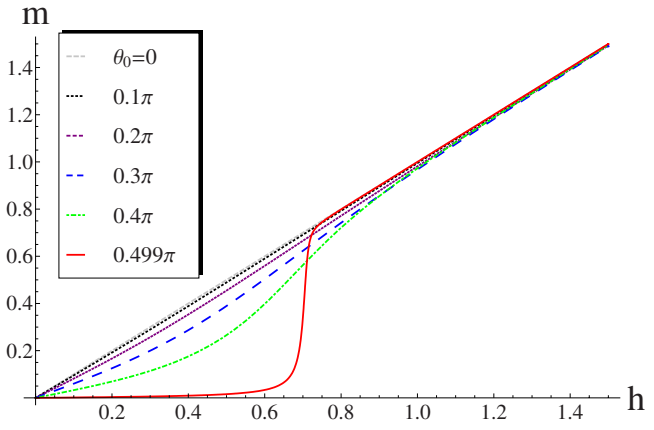

FIG. 5. (Color online) Magnitude of the magnetization m versus dimensionless field $\mathbf{h}$ for $\theta_h=0,0.1\pi,0.2\pi,0.3\pi,0.4\pi,0.499\pi$ (from the top curve to the bottom curve).

Before ending this section, we comment on the range of validity of the results. First, though we have assumed throughout the above that $c_1=0$, in fact it is possible to show that a spin flop (discontinuous jump in the magnetization) occurs throughout region I of the phase diagram in Fig. 3, in which $|c_1|<c_2$. For brevity, we do not give the (algebraically involved) argument here. Second, we have assumed a particular ordering wave vector along the (110) direction. At zero field, this wave vector is chosen spontaneously from among the family of equivalent $\langle 110\rangle$ planes [e.g., (101) etc.]. In the presence of a field, the different wave vectors will become inequivalent, due to the magnetic-anisotropy terms in f_{110}. Hence, given enough time, annealing, or field cycling, the system may choose the lowest free-energy wave vector among this set in the presence of the field. This is rather clearly the wave vector which is closest to the field axis. In this situation, the situation $\theta_h=\pi/2$ is avoided and the spin flop is avoided. In practice, wave-vector reorientation is probably sufficiently slow at low temperature to allow observation of the spin-flop transition.

IV. COMMENSURABILITY EFFECTS

Up to this point, our phenomenological theory leaves the *phase* of the spiral (i.e., the phase of $\mathbf{d}$) free. In general, the different directions within the spiral plane are not equivalent, and when a full account is taken of spin anisotropy and crystal symmetry, the phase of the spiral may take preferred values. In this section, we discuss the effects of "pinning" of the phase and how this leads to a lock-in transition for the spiral wave vector in some situations.

We will assume the spiral form in Eq. (2), with some given $\mathbf{q}(J_2/J_1)$ chosen to minimize the energy of the Heisen-

berg Hamiltonian. Using the arguments in Secs. II and III, we can fix the *plane* of the spiral, defined by the normal vector $\hat{\mathbf{e}}_3$. Choosing two *arbitrary* unit vectors spanning the plane ($\hat{\mathbf{e}}_1 \times \hat{\mathbf{e}}_2 = \hat{\mathbf{e}}_3$), we can then write

$$\mathbf{d} = m_s(\hat{\mathbf{e}}_1 + i\hat{\mathbf{e}}_2)e^{i\theta}. \tag{47}$$

The terms considered up to now do not fix the phase θ.

The freedom to choose θ is related to translational invariance. In particular, under a translation $\mathbf{r} \to \mathbf{r} + \mathbf{a}$, we have

$$\mathcal{T}_{\mathbf{a}}: \ \theta \to \theta - \mathbf{q} \cdot \mathbf{a}. \tag{48}$$

Here $\mathbf{a}$ can be any Bravais lattice vector. It is sufficient to consider the primitive lattice vectors $\mathbf{a} = (0, \frac{1}{2}, \frac{1}{2})$ and permutations. We would like to construct terms in the effective continuum Hamiltonian or Landau free energy that are invariant under Eq. (48) but which depend upon θ directly and not only through its gradients. Moreover, they must also be periodic in θ (since a shift by 2π leaves $\mathbf{d}$ unchanged). A general periodic functional of θ can be written,

$$V_\theta = -\sum_{n=1}^{\infty} \int d^3\mathbf{r} \lambda_n \cos[n\theta + \phi_n(\mathbf{r})], \tag{49}$$

where the λ_n are arbitrary coefficients. The ϕ_n are arbitrary *slowly varying functions* of $\mathbf{r}$, which should be chosen, if possible, to ensure invariance under Eq. (48). The functions should be slowly varying because large gradients of θ are heavily penalized by the Heisenberg Hamiltonian, which favors constant θ. If θ varies slowly but ϕ_n varies rapidly, then this term will average rapidly to zero on integration and can be neglected.

A general choice of function which achieves the desired invariance is $\phi_n(\mathbf{r}) = n\mathbf{q} \cdot \mathbf{r} (\mathrm{mod}\, 2\pi) + \phi_{n0}$, with ϕ_{n0} as a constant. We need to determine which (if any) of these functions is slowly varying. This occurs if the change in $\phi_n(\mathbf{r})$ on shifting by a primitive lattice vector is small. By continuity, this is achieved when $\mathbf{q}$ is close to a wave vector for which $\phi_n(\mathbf{r})$ is constant under such a shift. To achieve constancy, the nth term should have $n\mathbf{q} \cdot \mathbf{a}$, a multiple of 2π for all three primitive vectors $\mathbf{a}$. For this condition to hold for *any* n, we require that $\mathbf{q} \cdot \mathbf{a}$ be a rational multiple of 2π. We call these special wave vectors satisfying this condition *commensurate*.

Let us now specialize to a specific direction of wave vector of interest. We take $\mathbf{q} = (q, q, 0)$, corresponding to $J_2/J_1 \gtrsim 0.7$, which is the case appropriate for $MnSc_2S_4$. In this case, for the three primitive translations, we have $\mathbf{q} \cdot \mathbf{a} = q/2, q/2, q$. Thus the condition for the wave vector to be commensurate is $nq/2 = 2\pi m$, where n and m are integers. We assume that the system is close to such a value, i.e.,

$$q = 4 \arccos\left[\sqrt{\frac{|J_1|}{8J_2}}\right] \approx q_{m,n} \equiv \frac{4\pi m}{n}. \tag{50}$$

In general, the most important m, n will be those with the smallest n since the terms λ_n may be expected to decay with increasing n. For $J_2/J_1 \gtrsim 0.7$ such that the $(q, q, 0)$ order is obtained, we find a number of commensurate wave vectors, shown in Fig. 2. The smallest q in this set is $q = q_{3,8} = 3\pi/2$, which is the wave vector observed in $MnSc_2S_4$. The presence of these other commensurate wave vectors with smaller n suggests that other commensurate states might well be found by varying J_2/J_1 by physical or chemical pressure.

Let us fix on the vicinity of one of these wave vectors. Because the other terms in V_θ rapidly oscillate, we need only keep the one involving $q_{m,n}$:

$$V_\theta = -\lambda \int d^3\mathbf{r} \cos(n\theta + n\boldsymbol{\delta q} \cdot \mathbf{r} + \phi_{n0}), \tag{51}$$

where $\boldsymbol{\delta q} = \mathbf{q} - \mathbf{q}_{m,n}$, with $\mathbf{q}_{m,n} = (q_{m,n}, q_{m,n}, 0)$, and we simplified $\lambda_n \to \lambda$. This term favors configurations in which $\boldsymbol{\nabla}\theta = -\boldsymbol{\delta q} - \phi_{n0}$, which minimize the cosine. Establishment of a phase gradient, however, costs exchange energy. This can be seen because from Eqs. (2) and (47), a nonvanishing gradient $\boldsymbol{\nabla}\theta$ corresponds to a shift of wave vector. Indeed, the physical wave vector $\mathbf{k}$ for general θ is

$$\mathbf{k} = \mathbf{q} + \boldsymbol{\nabla}\theta. \tag{52}$$

The exchange energy cost of distorting the wave vector from $\mathbf{q}$ to $\mathbf{k}$ is, from Eq. (7),

$$H_{\mathrm{ex}} = \int d^3\mathbf{r} \frac{\kappa_{\mu\nu}}{2} \partial_\mu\theta\partial_\nu\theta, \tag{53}$$

where the tensor stiffness $\kappa_{\mu\nu}$ is

$$\kappa = \begin{pmatrix} \kappa_+ & \kappa_- & 0 \\ \kappa_- & \kappa_+ & 0 \\ 0 & 0 & \kappa_3 \end{pmatrix}. \tag{54}$$

Here $\kappa_1 = \kappa_+ + \kappa_-$, $\kappa_2 = \kappa_+ - \kappa_-$, and κ_3 are the stiffnesses along the principal axes. At zero temperature, they are given by

$$\kappa_1 = \frac{J_1}{2} - \frac{J_1^2}{16J_2} + \mathcal{O}[J_3],$$

$$\kappa_2 = \frac{(8J_2 - J_1)J_1J_3}{16J_2^2},$$

$$\kappa_3 = J_3 \frac{(128J_2^3 - 112J_1J_2^2 + 20J_1^2J_2 - J_1^3)}{8J_1J_2^2}. \tag{55}$$

For the most interesting case $q \approx 3\pi/2$, we have $\kappa_1 \approx (2 + \sqrt{2})J_1/8$, $\kappa_2 \approx J_3/2$, and $\kappa_3 \approx (\sqrt{2}+1)J_3$.

We now proceed to analyze the effective Hamiltonian $H_{\mathrm{eff}} = H_{\mathrm{ex}} + V_\theta$. Though we have given these expressions explicitly at $T=0$, the general form in Eqs. (51) and (53) holds at any temperature below the Néel temperature, with H_{eff} replaced by F_{eff}, the effective free energy, and with renormalized parameters $\lambda(T)$ and $\kappa_i(T)$. Moreover, because in this temperature range the system exhibits magnetic long-range order, the fluctuations of θ are small and bounded, so that it is sufficient to consider saddle points of the free energy.

It is convenient to shift variables to $\tilde{\theta} = \theta + \boldsymbol{\delta q} \cdot \mathbf{r} + \phi_{n0}/n$. The free energy is

$$F_{\text{eff}} = \int d^3\mathbf{r} \left\{ \frac{\kappa_{\mu\nu}}{2} \partial_\mu \tilde{\theta} \partial_\nu \tilde{\theta} + \boldsymbol{\delta} \cdot \boldsymbol{\nabla} \tilde{\theta} - \lambda \cos n\tilde{\theta} + \frac{1}{2} \delta q_\mu \kappa_{\mu\nu} \delta q_\nu \right\}, \tag{56}$$

with $\delta_\mu = \kappa_{\mu\nu} \delta q_\nu$. The last term is independent of $\tilde{\theta}$ and can be neglected. One can readily see that

$$\mathbf{k} = \mathbf{q}_{m,n} + \boldsymbol{\nabla} \tilde{\theta}. \tag{57}$$

The minimum free-energy saddle points of F_{eff} are translationally invariant along the directions perpendicular to $\boldsymbol{\delta}$, which is along the (110) axis. We therefore define the coordinate $\mathbf{x} = (x+y)/\sqrt{2}$ along the (110) direction, and rewrite the free energy accordingly,

$$F_{\text{eff}} = A \int d\mathbf{x} \left\{ \frac{\kappa_1}{2} (\partial_{\mathbf{x}} \tilde{\theta})^2 + \delta \partial_{\mathbf{x}} \tilde{\theta} - \lambda \cos n\tilde{\theta} \right\}, \tag{58}$$

where A is the area of the sample transverse to the (110) axis and $\delta = |\boldsymbol{\delta}| = q - q_{m,n}$, and we have dropped the constant term. It is now evident that δ enters only as a boundary term, which means that the free energy depends upon δ only through the "winding" number $N_w = [\tilde{\theta}(\mathbf{x}=L) - \tilde{\theta}(\mathbf{x}=0)] \frac{n}{2\pi}$ of the minimum-energy saddle point [across the length L along the (110) direction]. This allows one to proceed by finding the saddle-point energy for fixed N_w, and then minimizing over N_w.

It is useful to consider the cases $N_w = 0$ and $N_w = \pm 1$. For $N_w = 0$, the saddle point is uniform, $\tilde{\theta} = 0$ (up to a multiple of $2\pi/n$). For $N_w = \pm 1$, one has a single-soliton solution:

$$\tilde{\theta}(\mathbf{x}) = \frac{4}{n} \arctan[e^{\pm n\sqrt{\lambda/\kappa_1}(\mathbf{x}-\mathbf{x}_0)}], \tag{59}$$

where $\mathbf{x}_0$ is arbitrary and specifies the location of the center of the soliton. Note that the soliton width $w = \frac{1}{n}\sqrt{\frac{\kappa_1}{\lambda}}$. The energy of this solution, for $\delta = 0$, is $E_{N_w=1} - E_{N_w=0} = 8\sqrt{\kappa_1 \lambda}/n$. When the spacing between solitons is much larger than w, i.e., $L/|N_w| \gg w$, the energy of an N_w soliton state is approximately just $|N_w|$ times this single-soliton energy. Corrections to this noninteracting soliton approximation arise due to the overlaps of the exponential tails of the solitons. Defining the mean soliton density as $n_w = N_w/L$, we may then write the free-energy density as

$$f \sim \frac{8\sqrt{\kappa_1 \lambda}}{n} |n_w| + \frac{2\pi\delta}{n} n_w + c|n_w| e^{-1/w|n_w|}, \tag{60}$$

where c is a positive constant. From Eq. (60), the minimum n_w can be easily found. For $|\delta| < |\delta_c| = 4\sqrt{\kappa_1 \lambda}/\pi$, one has $n_w = 0$, and the wave vector is commensurate. For $|\delta| > |\delta_c|$, $n_w \neq 0$, and the wave vector becomes incommensurate. Due to fluctuations, one expects both λ and κ_1 to decrease with temperature. Hence the width of the commensurate state ($\propto |\delta_c|$) will decrease with increasing temperature. A schematic phase diagram is shown in Fig. 6.

We see that when J_2/J_1 is close (but not too close) to a value for which the Heisenberg model alone has a commensurate spiral solution, there is a lock-in transition on decreasing temperature from an incommensurate to a commensurate spiral. Within the commensurate ("C" in Fig. 6) phase, the wave vector is constant and equal to $q_{m,n}$. This is consistent with observations on $MnSc_2S_4$. Commensurate-incommensurate transitions of this type are well studied, and the reader interested in details of the associated critical behavior may find it in various standard texts, for instance, Ref. 8.

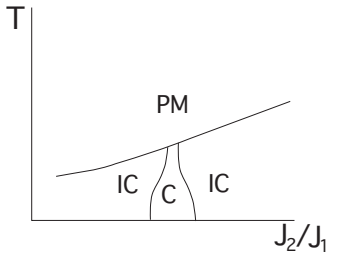

FIG. 6. Schematic phase diagram showing commensurate (C) and incommensurate (IC) magnetic phases and the paramagnetic (PM) phase. The figure is drawn as appropriate for a first-order magnetic transition line, in which case the width of the commensurate phase remains nonzero on approaching the Néel temperature.

V. QUANTUM FLUCTUATIONS

In this section, we develop a spin-wave theory for the diamond antiferromagnet, and obtain the leading quantum corrections to the spin correlations.

A. Holstein-Primakoff bosons

We proceed in the standard way by defining Holstein-Primakoff bosons in a spin coordinate frame rotated to follow the classical ordered state. The local orthonormal axes will be defined by

$$\hat{\mathbf{z}}_i = \hat{\mathbf{S}}_i^{\text{cl}} = \text{Re}[\mathbf{d} e^{i\mathbf{q}\cdot\mathbf{r}_i}],$$

$$\hat{\mathbf{x}}_i = -\text{Im}[\mathbf{d} e^{i\mathbf{q}\cdot\mathbf{r}_i}],$$

$$\hat{\mathbf{y}} = -\frac{i}{2} \mathbf{d} \times \mathbf{d}^* = \hat{\mathbf{e}}_3. \tag{61}$$

Note that the $\hat{\mathbf{y}}$ axis is site independent, as it just corresponds to the normal vector to the spiral plane. The linearized Holstein-Primakoff transformation is

$$\mathbf{S}_i = (S - n_i)\hat{\mathbf{z}}_i + \sqrt{2S} \left(a_i^\dagger \frac{(\hat{\mathbf{x}}_i + i\hat{\mathbf{y}})}{2} + a_i \frac{(\hat{\mathbf{x}}_i - i\hat{\mathbf{y}})}{2} \right), \tag{62}$$

which neglects corrections cubic in the canonical $a_i, a_i^\dagger$ boson operators. Here $n_i = a_i^\dagger a_i$ as usual. It is convenient to pass from canonical bosons to "coordinate" and "momentum" operators,

$$\chi_i = \frac{1}{\sqrt{2}}(a_i + a_i^\dagger), \quad \xi_i = i\frac{1}{\sqrt{2}}(a_i^\dagger - a_i). \tag{63}$$

The spin operator becomes

$$\mathbf{S}_i = (S - n_i)\hat{\mathbf{z}}_i + \sqrt{S}(\chi_i \hat{\mathbf{x}}_i + \xi_i \hat{\mathbf{y}}), \tag{64}$$

and

$$n_i = \frac{\chi_i^2}{2} + \frac{\xi_i^2}{2} - \frac{1}{2}. \tag{65}$$

B. Spin-wave Hamiltonian

Inserting Eq. (64) into the Heisenberg Hamiltonian, we obtain terms of $\mathcal{O}(S^2)$, $\mathcal{O}(S^{3/2})$, and $\mathcal{O}(S)$, dropping higher-order corrections:

$$H_{\mathcal{O}(S^2)} = \frac{1}{2} S^2 J_{ij} \hat{\mathbf{z}}_i \cdot \hat{\mathbf{z}}_j,$$

$$H_{\mathcal{O}(S^{3/2})} = \frac{S\sqrt{S}}{2\sqrt{2}} J_{ij} \hat{\mathbf{z}}_i \cdot \hat{\mathbf{z}}_i (\chi_i + \chi_j),$$

$$H_{\mathcal{O}(S)} = \frac{1}{2} S J_{ij} [(n_i + n_j)\hat{\mathbf{z}}_i \cdot \hat{\mathbf{z}}_j + \chi_i \chi_j \hat{\mathbf{x}}_i \cdot \hat{\mathbf{x}}_j + \xi_i \xi_j]. \tag{66}$$

The $\mathcal{O}(S^{3/2})$ term vanishes because the local coordinate vectors are eigenstates of the exchange matrix, e.g.,

$$J_{ij} \hat{\mathbf{z}}_j = J_m \hat{\mathbf{z}}_i, \tag{67}$$

and $\hat{\mathbf{x}}_i \cdot \hat{\mathbf{z}}_i = 0$. Here J_m is the minimum eigenvalue of the exchange matrix. The vanishing of the $O(S^{3/2})$ term is of course true because we expand about the classical ground state.

Using Eq. (67), one can further simplify the spin-wave Hamiltonian. We obtain

$$H_{\mathcal{O}(S)} = -\sum_i \frac{S J_m}{2} (\chi_i^2 + \xi_i^2) + \sum_{ij} \frac{S J_{ij}}{2} (\chi_i \chi_j \hat{\mathbf{x}}_i \cdot \hat{\mathbf{x}}_j + \xi_i \xi_j), \tag{68}$$

neglecting constant terms which do not affect the correlations.

C. Action

Spin fluctuations are conveniently calculated using the path-integral approach. The imaginary time action corresponding to Eq. (68) has the usual Berry phase terms describing the canonical commutation relations of χ_i and ξ_i,

$$S = \int_\tau \left\{ H_{\mathcal{O}(S)} + \sum_i i \chi_i \partial_\tau \xi_i \right\}. \tag{69}$$

Static correlations of χ_i and ξ_j vanish, so we may consider the two separately. It is then convenient to integrate out one of these fields to obtain an effective action for the other. This gives

$$S_\chi = \frac{1}{2} \sum_{ij} \int_\tau \left\{ S \widetilde{K}_{ij} \chi_i \chi_j + \frac{1}{S} [\widetilde{J}^{-1}]_{ij} \partial_\tau \chi_i \partial_\tau \chi_j \right\}, \tag{70}$$

$$S_\xi = \frac{1}{2} \sum_{ij} \int_\tau \left\{ S \widetilde{J}_{ij} \xi_i \xi_j + \frac{1}{S} [\widetilde{K}^{-1}]_{ij} \partial_\tau \xi_i \partial_\tau \xi_j \right\}, \tag{71}$$

where

$$\widetilde{J}_{ij} = J_{ij} - J_m \delta_{ij}, \tag{72}$$

$$\widetilde{K}_{ij} = J_{ij} \hat{\mathbf{x}}_i \cdot \hat{\mathbf{x}}_j - J_m \delta_{ij}. \tag{73}$$

To diagonalize this, we move to momentum space. Due to the sublattice structure, we define two components for each field, $\chi_{A\mathbf{k}}$, $\chi_{B\mathbf{k}}$ and $\xi_{A\mathbf{k}}$, $\xi_{B\mathbf{k}}$, such that

$$\chi_i = \int_{\mathbf{k}} \chi_{s(i)\mathbf{k}} e^{i\mathbf{k}\cdot\mathbf{r}_i}, \tag{74}$$

$$\xi_i = \int_{\mathbf{k}} \xi_{s(i)\mathbf{k}} e^{i\mathbf{k}\cdot\mathbf{r}_i}, \tag{75}$$

where $s(i) = A, B$ specifies the diamond sublattice of the site i. The $\mathbf{k}$ integral is defined as $\int_{\mathbf{k}} = v_{\mathrm{uc}} \int \frac{d^3\mathbf{k}}{(2\pi)^3}$, where the integration domain is the first Brillouin zone, and $v_{\mathrm{uc}} = 1/4$ is the volume of the real space unit cell. It is convenient to define

$$\hat{\chi}_{\mathbf{k}} = \begin{pmatrix} \chi_{A\mathbf{k}} \\ \chi_{B\mathbf{k}} \end{pmatrix}, \quad \hat{\xi}_{\mathbf{k}} = \begin{pmatrix} \xi_{A\mathbf{k}} \\ \xi_{B\mathbf{k}} \end{pmatrix}. \tag{76}$$

The action becomes

$$S_\chi = \frac{1}{2} \int_{\mathbf{k}\omega} \hat{\chi}^T_{-\mathbf{k},-\omega} \cdot \overleftrightarrow{G}^{-1}_\chi(\mathbf{k},\omega) \cdot \hat{\chi}_{\mathbf{k},\omega}, \tag{77}$$

$$S_\xi = \frac{1}{2} \int_{\mathbf{k}\omega} \hat{\xi}^T_{-\mathbf{k},-\omega} \cdot \overleftrightarrow{G}^{-1}_\xi(\mathbf{k},\omega) \cdot \hat{\xi}_{\mathbf{k},\omega}. \tag{78}$$

Here the frequency integral is $\int_\omega = \int \frac{d\omega}{2\pi}$ as usual. The matrix Green's functions are straightforwardly found but somewhat cumbersome. The reader interested in the details is referred to Appendix B. With all these definitions, one can formally evaluate the equal-time correlation functions:

$$\langle \chi_i \chi_j \rangle = \int_{\mathbf{k},\omega} [G_\chi(\mathbf{k},\omega)]_{s(j)s(i)} e^{i\mathbf{k}\cdot(\mathbf{r}_i - \mathbf{r}_j)},$$

$$\langle \xi_i \xi_j \rangle = \int_{\mathbf{k},\omega} [G_\xi(\mathbf{k},\omega)]_{s(j)s(i)} e^{i\mathbf{k}\cdot(\mathbf{r}_i - \mathbf{r}_j)}. \tag{79}$$

Here the subscripts give the matrix elements of the matrix Green's functions.

D. Local moment

Focusing on the case of $MnSc_2S_4$, with $\mathbf{q} = (3\pi/2, 3\pi/2, 0)$, we have calculated the reduction in the sublattice magnetization by numerically evaluating the momentum integrals in Eq. (79) (the frequency integration can be done analytically). See Appendix C for more details of the calculation. The result for the on-site expectation value is

$$\langle \chi_i^2 \rangle \approx 0.67, \quad \langle \xi_i^2 \rangle \approx 1.19, \tag{80}$$

for $J_3 = 0.1K \approx J_1/100$. From this, one obtains $\langle n_i \rangle \approx 0.43$ from Eq. (65), which is approximately a 20% reduction from

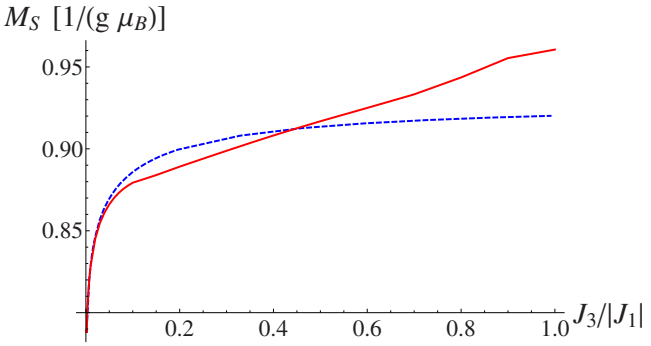

FIG. 7. (Color online) Reduced magnetic moment M_s as a function of $J_3/|J_1|$. The solid line is for fixed J_2, while the dashed line is for J_2, J_3 satisfying Eq. (11), so that the wave vector remains equal to $3\pi/2(1,1,0)$.

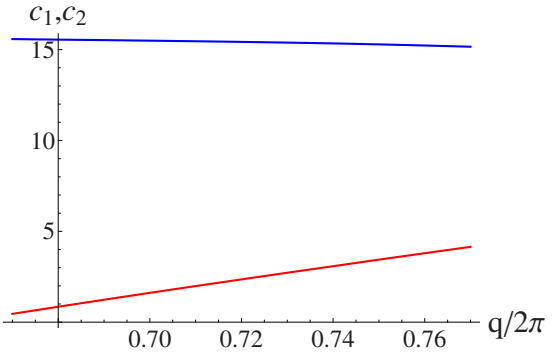

FIG. 8. (Color online) Calculated anisotropy parameters (in arbitrary units) c_1 (upper curve) and c_2 for $\mathbf{q}=(q,q,0)$ as a function of $q/(2\pi)$.

the classical local moment. As J_3 is increased, the moment increases closer to the classical value, as shown in Fig. 7.

VI. MICROSCOPIC ORIGIN OF MAGNETIC ANISOTROPY

In Secs. II B and III, we studied the effects of explicit spin-rotation symmetry breaking on *phenomenological* grounds, using only the space-group symmetry of spinel structure. In this section, we address its microscopic origins. There are in general two mechanisms of spin-rotation symmetry violation in solids: (1) dipole interactions between electron spins, and (2) spin-orbit coupling. We consider both in turn and find these lead to somewhat different regimes of the phenomenological model discussed previously. Interestingly, only the spin-orbit coupling mechanism can explain the observations in $MnSc_2S_4$.

A. Dipolar interactions

The dipole-dipole interaction can be written as

$$\mathbf{H}_D = \frac{\mu_0}{4\pi}\sum_{i,j}\frac{\mathbf{m}_i\cdot\mathbf{m}_j}{r_{ij}^3} - \frac{3\mathbf{m}_i\cdot\mathbf{r}_{ij}\mathbf{m}_j\cdot\mathbf{r}_{ij}}{r_{ij}^5}, \tag{81}$$

where $\mathbf{m}_i = g\mu_B S\mathbf{S}_i$ is the dipole moment of the spin i (we included an explicit factor of S to follow our convention of unit vector spins). Using $g\approx 2$ as expected for an $S=5/2$ Mn^{2+} spin with a half-filled d shell, we obtain a dipolar energy of interaction between two nearest-neighbor spins of approximately $0.5K$. We note that this is not negligible (especially when added over many spins within a correlation volume) but it is certainly weak compared to the basic energy scale of exchange interactions as estimated from the Curie-Weiss temperature $\Theta_{CW}\approx -23$ K. Therefore we expect we can treat the dipolar interaction as a weak (but symmetry-breaking) perturbation on the ordered ground states of the Heisenberg model.

To this end, we first consider the dipolar interaction classically by simply inserting the general spiral form of Eq. (29) into Eq. (81) and evaluating the sum. Because we are only interested in the dependence of the energy upon the spin orientation of the spiral, we may drop the first term in Eq. (81), which is fully SU(2) invariant. Because the spiral itself is at a nonzero wave vector, there are no convergence difficulties with the long-range dipolar sum. Choosing the wave vector $\mathbf{q}=(q,q,0)$ as in experiment, one indeed finds the form in Eq. (22) is obtained provided the sum is truncated in a manner preserving cubic symmetry. We plot the values of c_1 and c_2 in Eq. (27) in the physical range of q for $0.7 \lesssim J_2/J_1 < 1$ in Fig. 8. Throughout this range we find $c_1 > 0$ and more than three times as large as c_2. This favors alignment of spins within the plane normal to $\hat{\mathbf{e}}_3=(110)$. Unfortunately, this is *not* what is found experimentally.

Several possible complications should be considered before abandoning dipolar interactions as a mechanism of magnetic anisotropy. First, in applying Eq. (81) with $\mathbf{m}_i = g\mu_B S\mathbf{S}_i$, we have treated the electron spins as point dipoles. In fact, the electronic wave functions may be somewhat extended. Through such "covalency," there may be some spin density not only in the atomic d orbital of the Mn^{2+} ion but also on the neighboring chalcogenide p orbitals. This can be approximately accounted for by modifying the dipole-moment distribution associated with a spin accordingly, to be distributed among with a fractional moment $1-f$ on the central Mn^{2+} ion and a fraction $f/4$ on each of the neighboring four S^{2-} ions. We have carried out such a modified dipolar sum, and found that it does not substantially alter the results of the point-dipole model for a reasonable range of parameters f.

Another more interesting possibility is that fluctuations may alter the dipolar energetics. This is not an unreasonable possibility to consider since, although the classical order-parameter description is expected to qualitatively (and indeed rather quantitatively) capture the long-range order of the spins, the dipolar energy actually receives large contributions from very near spins. The latter could exhibit quite different correlations from well-separated spins which control the order parameter.

To consider this effect, we have calculated the leading corrections in $1/S$ to the dipolar energy using the spin-wave formalism described in Sec. V. Since we treat the dipole-dipole interaction as a perturbation, it is sufficient to consider the expectation value $\langle H_D\rangle$ in each of the spin-wave ground states specified by $\mathbf{d}$. To do so, we insert Eq. (64) into H_D and expand to quadratic order in χ_i and ξ_i, then take the

TABLE I. Numerically calculated values of correlations of ξ_i and χ_i fields from spin-wave theory, for $\mathbf{q}=(3\pi/2,3\pi/2,0)$, $J_2/J_1=\frac{1}{8}\cos^2(\pi/8)$, and $J_3/J_1=0.01$. Values not specified have negligible correlations.

$\mathbf{r}_{ij}$	$\langle\chi_i\chi_j\rangle$	$\langle\xi_i\xi_j\rangle$
0	0.67	1.19
$\pm 1/2(1,1,0)$	0.22	−0.1
$1/2(\pm 1,0,\pm 1)$	0.18	−0.3
$1/4\ (1,1,-1)$	−0.25	0.23
$-1/4(1,1,1)$	−0.25	0.23

expectation value of the result. The necessary correlators of χ_i and ξ_i are calculated by numerical integration of Eq. (79). The values obtained are given in Table I. Because the basis vectors $\hat{\mathbf{x}}_i$, $\hat{\mathbf{y}}$, and $\hat{\mathbf{z}}_i$ are expressed in terms of $\mathbf{d}$ in Eq. (61), the result is again an energy function of the form of Eq. (27), which contains both the classical expressions for c_1 and c_2 and their leading quantum corrections. We find that the quantum corrections push the system even further from the $\hat{\mathbf{e}}_3=(110)$ state, and in any case the magnitude of the corrections is very small compared to the classical values.

Having thus exhausted the possible complications associated with the dipolar interactions, we conclude that the observed ordered state in $MnSc_2S_4$ is inconsistent with a dipolar origin of the magnetic anisotropy. We therefore turn to spin-orbit effects in Sec. VI B.

B. Exchange anisotropy due to spin-orbit coupling

As we saw in Sec. VI A, dipolar interactions do not appear to be viable explanation of the orientation of the spin spiral observed in $MnSc_2S_4$. We now consider the second microscopic origin of magnetic anisotropy, which is spin-orbit coupling. From the point of view of symmetry, the spinel lattice allows both single-ion (cubic) anisotropy of the Mn^{2+} spins and exchange anisotropy. The former is however expected to be extremely small for Mn^{2+}, which has an extremely stable and isotropic $3d^5$ configuration (one may expect a coupling constant of a few *millikelvins*). However, exchange anisotropy is non-negligible in many Mn magnets. A microscopic calculation is beyond the scope of this paper, but we can make a few statements on general grounds. Because of the closed-shell configuration, these effects are also expected to be much smaller than the typical exchange interactions (i.e., perturbative in spin-orbit coupling). However, they may still be as large as or larger than the dipolar effects. In $MnSc_2S_4$, one may attempt to get some feeling for their magnitude by comparing the measured effective moment seen in the Curie law $\mu_{\text{eff}}=5.8\mu_B$ to the theoretical spin-only value $\mu_{S=5/2}=2\sqrt{\frac{5}{2}\frac{7}{2}}\approx 5.92$. Given uncertainties in the measurement, we expect no more than a 5–10 % deviation from the latter (and very possibly much better agreement masked by experimental complications). For Mn^{2+}, one expects that contributions to the g factor (which renormalize the effective moment) are *second order* in the spin-orbit coupling. Exchange anisotropy occurs at both first order and second order. At first order, one obtains the antisymmetric Dzyaloshinskii-Moriya (DM) interaction, and at second order, symmetric exchange anisotropy. Thus we would expect that the DM interactions be of order $\sqrt{|\mu_{\text{eff}}-\mu_{5/2}|/\mu_{5/2}}J_{ij}$ and symmetric exchange anisotropy be of order $(|\mu_{\text{eff}}-\mu_{5/2}|/\mu_{5/2})J_{ij}$.

With this in mind, we consider the allowed *form* of the exchange anisotropy as constrained by the space-group symmetry of the spinel structure. We first consider nearest-neighbor bonds. Without loss of generality, take a bond oriented along the (111) axis. DM interaction is *forbidden* on this bond because exactly between the two sites is an inversion center [$\mathcal{G}_5$ in Eq. (17)]. Thus we need only consider exchange anisotropy. This in turn is strongly constrained by the C_3 rotation symmetry about the (111) axis [$\mathcal{G}_3$ in Eq. (17)]. This allows only two separate exchange couplings, for components parallel and perpendicular to the bond. We can write the associated exchange Hamiltonian as

$$H_{\text{ani}}^{\text{nn}}=\sum_{\langle i,j\rangle} J_{\parallel}\mathbf{n}_{ij}\cdot\mathbf{S}_i\mathbf{n}_{ij}\cdot\mathbf{S}_j+J_{\perp}\mathbf{n}_{ij}\times\mathbf{S}_i\cdot\mathbf{n}_{ij}\times\mathbf{S}_j. \quad (82)$$

There is a single parameter, $J_{\perp}-J_{\parallel}$, which parametrizes the nearest-neighbor exchange anisotropy.

Next, we consider the exchange anisotropy for next-nearest neighbors. Here the symmetry is considerably less constraining since two second neighbors (fcc neighbors) are not connected by a C_3 axis, and there is no inversion center between them. We have however determined the most general exchange Hamiltonian between two such sites invariant under all operations in Eq. (17), which is a straightforward but tedious calculation. There is unfortunately no simple expression for this Hamiltonian which describes all six second-neighbor bonds simultaneously. Instead we write the form for a particular bond, connecting two sites i and j on the "A" sublattice, separated by the (arbitrarily chosen) Bravais lattice vector $\mathbf{r}_{ij}=(0,-\frac{1}{2},\frac{1}{2})$:

$$H_{ij}^{\text{nnn}}=J_aS_i^xS_j^x+D(S_i^xS_j^y-S_i^yS_j^x+S_i^xS_j^z-S_i^zS_j^x)+J_b(S_i^yS_j^z+S_i^zS_j^y)+J_c(S_i^yS_j^y+S_i^zS_j^z). \quad (83)$$

The full set of H_{ij} for all other pairs of second-neighbor sites can be obtained by actions of symmetry operations on Eq. (83), which thus defines the full next-nearest-neighbor Hamiltonian $H_{\text{ani}}^{\text{nnn}}$. Note that there are three symmetric exchange constants, one linear combination of which represents the isotropic Heisenberg term, and the other two (J_b and J_a-J_c) represent symmetric exchange anisotropy. Because of the absence of an inversion center between two fcc sites in the spinel, there is an allowed DM term D. However, the presence of the inversion center implies that the D term takes the opposite sign for spins on the "B" sublattice.

We can now consider the full exchange-anisotropy Hamiltonian, $H_{\text{ani}}=H_{\text{ani}}^{\text{nn}}+H_{\text{ani}}^{\text{nnn}}-H_{\text{Heis}}$, as a perturbation to the Heisenberg form, and evaluate the energy splittings induced for a given spiral state specified by $\mathbf{q}$ and $\mathbf{d}$, by simply inserting Eq. (2) into H_{ani}. As required by symmetry, for $\mathbf{q}=(qq0)$ it again has the form of Eq. (22). Reading off the coupling constants, we find

$$c_1 = (J_a - J_c)(1 + \sqrt{2}) + \left(1 - \frac{1}{\sqrt{2}}\right)(J_\perp - J_\parallel),$$

$$c_2 = J_b. \tag{84}$$

Note that the DM term D does not enter these macroscopic anisotropy parameters, which is a consequence of its staggered nature on the two diamond sublattices.

Unlike for the dipolar interactions, we see that Eq. (84) allows essentially arbitrary values of c_1 and c_2. This means that in the absence of a microscopic calculation, the exchange-anisotropy mechanism is not inconsistent with the observed ordering in $MnSc_2S_4$, which as we saw could be described phenomenologically by a range of choices of c_1 and c_2. Given the *incompatibility* of our dipolar results, however, we tentatively conclude that spin-orbit-induced exchange anisotropy is likely at the origin of spin-state selection in $MnSc_2S_4$.

VII. DISCUSSION

A. Summary

In this paper, we have extended the theory of Ref. 6 to describe the effects of magnetic anisotropy and quantum fluctuations in frustrated antiferromagnetic A-site spinels. The theory predicts the possible planes on which spins reside in the spiral magnetic ground states in zero field, and describes their evolution with field. In some orientations a spin-flop transition was found. We described commensurate-incommensurate transitions which occur below the Néel temperature when the spiral wave vector locks to one of a set of specific commensurate values. These effects are all in accord with observations on the best studied such material, $MnSc_2S_4$. We addressed the reduced static moment seen in $MnSc_2S_4$ by spin-wave calculations, and found that a relatively large reduction can indeed be achieved by quantum fluctuations due to the frustration-induced degeneracy, despite the large $S=5/2$ spin of Mn^{2+}, if one assumes the third-neighbor exchange $J_3 \lesssim 0.1$. Finally, we derived microscopic expressions for the most important phenomenological magnetic-anisotropy parameters, taking into account both dipole-dipole interactions and spin-orbit effects. In $MnSc_2S_4$, we concluded that the latter are most likely responsible for the observed magnetic orientation.

B. Experiments

Let us turn now to a further discussion of experiments. First we discuss existing results and then consider future experiments.

1. Local moment

As mentioned above, from the weight in the magnetic Bragg peaks seen in Ref. 7 in $MnSc_2S_4$, it was estimated that the local ordered moment $M_s \approx 0.8 M_{cl}$, where M_{cl} is the expected classical static moment for an $S=5/2$ spin. In Sec. V D, we showed that the 17% reduction could perhaps be due to quantum fluctuations if J_3 is sufficiently small. However, there are a number of reasons to be cautious about this conclusion. First, at a technical level, it is not clear to us how large the experimental errors should be considered on this measurement, which was done in a powder sample. Second, the data were taken at $T=1.5$ K, more than half the ordering temperature $T_c=2.3$ K, so thermal fluctuations may contribute to some reduction in the moment.

Finally, there are a number of different effects that have not been addressed theoretically, which may contribute to the moment reduction. First, we have neglected disorder, which is known to be present in the form of inversion—interchange of A- and B-site atoms of the spinel. Such disorder can damage the spin spiral, reducing the *ordered* moment even if the local static moments remain large. The nature of the defects created and their impact on the ordered moment measured by neutrons will be discussed in a separate future work.[9] A second effect that could contribute is a spin-orbit renormalization of the g factor. Usually this is small in Mn^{2+} magnets, but perhaps this is something worth considering further.

2. Microscopics of anisotropy

As discussed above and in Sec. VI, though dipolar interactions between Mn^{2+} spins might seem a likely candidate for the origin of the magnetic anisotropy in $MnSc_2S_4$, they appear to be inconsistent with the observed nature of this anisotropy. While we can reconcile the existing experiments with a picture of spin-orbit-induced anisotropy (with some assumptions), it is still surprising to us that such effects would be competitive with dipolar interactions. We believe the conflict of the latter with the ordered state seen in $MnSc_2S_4$ is a significant one, and found in Sec. VI A that neither covalency nor quantum fluctuations were likely to effect a reconciliation.

One possibility we have *not* considered is the effect of disorder and granularity. Given the long-range nature of the dipolar interaction, it is possible that defects created by disorder in an ideal spiral can facilitate large changes in the dipolar energy. This is an interesting issue to be explored in the future. We emphasize that, although such a mechanism of anisotropy might be possible, the phenomenological portion of our theory is entirely independent of these details and is quite generally valid irrespective of the microscopic physics of anisotropy.

3. Magnetization experiments

We now turn to future experiments. Of particular interest would be the development of single crystals. This was already emphasized in Ref. 6, where predictions were made for unusual spiral-surface structure in the angle-resolved neutron structure factor. Based on the results of this paper, we suggest that single crystals are also interesting for the study of magnetization effects. An obvious suggestion is to look for signs of the spin-flop transition discussed in Sec. III B. Another interesting measurement would be torque magnetometry. As shown in Fig. 9, the angle of the magnetization can be strongly misaligned with the applied field, which should lead to a large torque. This is a very sensitive technique that perhaps does not require crystals as large as those for neutron scattering.

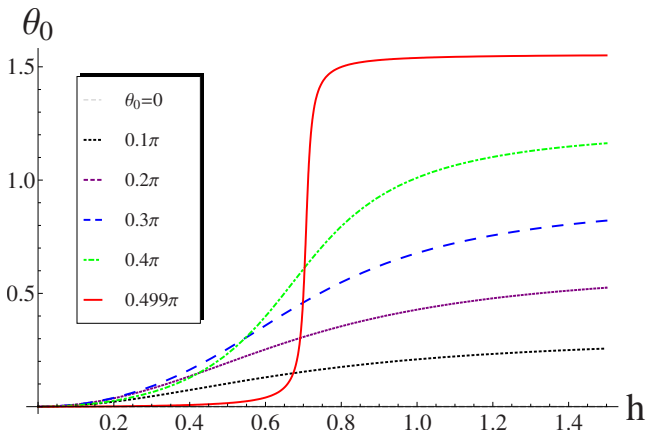

FIG. 9. (Color online) Ground-state angle θ_0 of the magnetization versus field $\mathbf{h}$ for $\theta_h=0,0.1\pi,0.2\pi,0.3\pi,0.4\pi,0.499\pi$ (from the bottom curve to the top curve).

C. Ferroelectricity

Our results enable us to discuss magnetically induced ferroelectricity in the *A*-site spinels. This may be expected since many recent studies, both theoretical and experimental, have emphasized the relation between spiral spin states and ferroelectricity. The basis for such a relationship goes back much earlier to symmetry considerations of Landau and Lifshitz[10] and Dzyaloshinskii.[11] Several recent studies have pointed out that very general arguments suggest a simple relationship between the electric polarization $\mathbf{P}$ and the basic parameters $\hat{\mathbf{e}}_3$ and $\mathbf{q}$ describing the spiral:[12–14]

$$\mathbf{P} \propto \mathbf{e}_3 \times \mathbf{q}. \tag{85}$$

Here, as in the text, $\hat{\mathbf{e}}_3$ is the axis which is perpendicular to the plane of the spins and $\mathbf{q}$ is the wave vector.

The argument leading to Eq. (85) is rather simplified and actually assumes a sort of "spherical symmetry." In reality, in the reduced crystal symmetry environment of the solid, the actual relation may be somewhat different. Still, for the *A*-site spinels, a complete symmetry analysis leads to rather similar results. In particular, time-reversal symmetry allows a quadratic term in the $\mathbf{d}$ order parameter (which is time-reversal odd) to couple linearly to $\mathbf{P}$. One therefore expects the polarization to take the form

$$P_\alpha = c_{\alpha\beta\gamma}(\mathbf{q}) d^*_\beta d_\gamma. \tag{86}$$

As argued earlier, all such bilinears in $\mathbf{d}$ can be rewritten in terms of $\hat{\mathbf{e}}_3$. The coefficients $c_{\alpha\beta\gamma}$ are constrained by crystal symmetry. Specifically, we require that the left- and right-hand sides of Eq. (86) transform identically under the little group which leaves $\mathbf{q}$ invariant.

For $\mathbf{q}=(q,q,q)$, applying Eq. (19), we find the form

$$\mathbf{P}_{111} = c_1 \begin{pmatrix} e_3^x \\ e_3^y \\ e_3^z \end{pmatrix} + c_2 \begin{pmatrix} e_3^z \\ e_3^x \\ e_3^y \end{pmatrix} + c_3 \begin{pmatrix} e_3^y \\ e_3^z \\ e_3^x \end{pmatrix}. \tag{87}$$

The simplified Eq. (85) corresponds to $c_1=0$, $c_3=-c_2$. However, in general, symmetry allows any values of c_1, c_2, and c_3.

For $\mathbf{q}=(q,q,0)$, using Eq. (20), we find instead

$$\mathbf{P}_{110} = c_1 \begin{pmatrix} e_3^z \\ -e_3^z \\ 0 \end{pmatrix} + c_2 \begin{pmatrix} 0 \\ 0 \\ e_3^x - e_3^y \end{pmatrix}. \tag{88}$$

Equation (85) is the special case $c_2=-c_1$.

Given these results, we can make some limited predictions on the ferroelectric polarization in the *A*-site spinels. In $MnSc_2S_4$, where the ordering wave vector and spiral plane is known, we can directly apply Eq. (88) without much ambiguity. We have $\hat{\mathbf{e}}_3=\hat{\mathbf{z}}$, which means that there is a spontaneous polarization with $\mathbf{P}$ along the $1\bar{1}0$ direction. It would be interesting to search for this experimentally in single crystals or for dielectric anomalies related to this in powders. Moreover, the phenomenological theory in Sec. III B, in conjunction with Eq. (88), describes how this polarization may be rotated by an applied field. Again, detailed single-crystal studies would be enlightening.

For spinels in the regime where $\mathbf{q}=(q,q,q)$, the theory is somewhat less predictive. This is because not only is there ambiguity in the spiral plane giving $\hat{\mathbf{e}}_3$ [due to the unknown constant c in Eq. (26)], but also there are more unknowns in the relation between the polarization and the spiral plane [Eq. (87)]. A microscopic theory for Eq. (87), which determines the c_i, is therefore desirable. We imagine one might be constructed based on the inverse Dzyaloshinskii-Moriya interaction mechanism[13] since we have seen that there is a single DM interaction allowed in the *A*-site spinels—see Eq. (83). The polarization can be very sensitive to details of the microscopics. For instance, for $c>0$ in Eq. (26), we have $\hat{\mathbf{e}}_3=(1,1,1)/\sqrt{3}$, and according to Eq. (85), the polarization *vanishes*. However, in general this is an artifact of the simplifications in Eq. (85), and according to Eq. (87), $\mathbf{P}\neq 0$. However the orientation of the polarization is precisely controlled by deviations from the naïve Eq. (85).

ACKNOWLEDGMENTS

The authors would like to thank A. Loidl, A. Krimmel, and M. Mücksch for discussions and correspondence. This research was supported by the Packard Foundation and the National Science Foundation through Grant No. DMR04-57440.

APPENDIX A: SPLITTING OF SPIRAL-SURFACE DEGENERACY

In this appendix, we give some details on how the ground-state spirals are determined in the presence of third-neighbor antiferromagnetic exchange J_3. First, we performed a numerical study of the minima of Eq. (10), considering only wave vectors fixed on the spiral surface, i.e., satisfying $\Lambda(\mathbf{k})=\lambda=1/8J_2$. These can be conveniently studied by solving this condition to give k_z in terms of k_x and k_y:

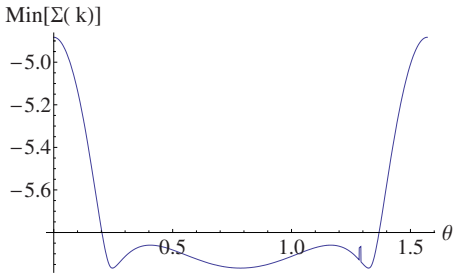

FIG. 10. (Color online) Minimum value of $\Sigma(\mathbf{k})$ for $\mathbf{k}$ of the form $\mathbf{k}=(q\cos\theta, q\sin\theta, k)$ as a function of θ, for $J_2/J_1=0.4$. For *all* values of J_2/J_1, the minimum value is achieved at $\theta=\pi/4$.

$$k_z = \pm 4\arccos\left[\left(\frac{\lambda^2 - \sin^2\frac{k_x}{4}\sin^2\frac{k_y}{4}}{\cos^2\frac{k_x}{4}\cos^2\frac{k_y}{4} - \sin^2\frac{k_x}{4}\sin^2\frac{k_y}{4}}\right)^{1/2}\right]. \tag{A1}$$

Here the solution (and the surface) exists only when the argument of the square root is between 0 and 1. Inserting this value of k_z into Eq. (10), we can obtain the energy on the surface explicitly. One can then scan linearly along lines defined by $\mathbf{k}=(q\cos\theta, q\sin\theta, k)$ on the surface and determine the lowest energy for each θ. In every case, the lowest energy as a function of θ is achieved for $\theta=\pi/4$ (an example is shown in Fig. 10), which implies a wave vector of the form (q,q,k) on the surface.

Having determined that the ground-state wave-vector is always of the (q,q,k) form, we need only search this ray for the ground state. This can be done analytically. One obtains

$$\begin{aligned}\Sigma(q) &\equiv \Sigma[q,q,k_z(q)] \\ &= \frac{1}{64}[96(8\lambda^2-3)\lambda^2 + (256\lambda^4-13)\cos q \\ &\quad + 2(16\lambda^2+5)\cos 2q - 3\cos 3q + 6]\sec^2\frac{q}{2}.\end{aligned} \tag{A2}$$

This should be evaluated only when such a wave vector exists on the surface. This condition is

$$\sin^2\frac{q}{4} < \lambda \quad \text{or} \quad \sin^2\frac{q}{4} > 1-\lambda. \tag{A3}$$

Now it is simple to study the ground states. One can check that the (q,q,q) state, for which $q=\arccos[(8\lambda^2-5)/3]$, is always a local minimum of Eq. (A2). It, however, only exists when this value is well defined, which requires $\lambda > 1/2$. This corresponds to $1/4 < J_2 < 1/2$. Indeed, in this range it is straightforward to show that this is the global energy minimum.

For J_2 sufficiently large, one can readily see that the minimum of Eq. (A2) is instead achieved at the boundary of its domain of validity, i.e., when the inequalities in Eq. (A3) are satisfied as *equalities*. This corresponds to $k_z(q)=0$, i.e., a $(q,q,0)$ state. This eventually ceases to be a minimum for small enough J_2. A choice of such wave vector is $q=q_0=4\arcsin\sqrt{\lambda}$. For this to be a minimum, we need $\Sigma'(q_0)<0$. By differentiating Eq. (A2) and evaluating, we find

$$\Sigma'(q_0) = 16[\lambda(1-\lambda)]^{3/2}\frac{1-6\lambda+4\lambda^2}{2\lambda-1}. \tag{A4}$$

It is straightforward to show that this is negative provided $\lambda < (3-\sqrt{5})/4$ or $J_2 > 1/[2(3-\sqrt{5})]$, which determined the domain of the $(q,q,0)$ state. In between this and the (q,q,q) state, we necessarily have the (q,q,q^*) state.

APPENDIX B: SPIN-WAVE GREEN'S FUNCTIONS

In this appendix, we give some details of the spin-wave Green's functions. The Green's functions defined in Eq. (77) can be written as

$$\overleftrightarrow{G}_\chi(\mathbf{k},\omega) = \{\overleftrightarrow{SB}(\mathbf{k}) + \omega^2[\overleftrightarrow{SA}(\mathbf{k})]^{-1}\}^{-1}, \tag{B1}$$

$$\overleftrightarrow{G}_\xi(\mathbf{k},\omega) = \{\overleftrightarrow{SA}(\mathbf{k}) + \omega^2[\overleftrightarrow{SB}(\mathbf{k})]^{-1}\}^{-1}. \tag{B2}$$

Here we have defined a number of matrices occurring as Fourier transforms of exchange matrices:

$$\overleftrightarrow{A}(\mathbf{k}) = \overleftrightarrow{W}_{\mathbf{q},\gamma}(\mathbf{k}), \quad \overleftrightarrow{B}(\mathbf{k}) = \overleftrightarrow{W}_{0,0}(\mathbf{k}), \tag{B3}$$

$$\overleftrightarrow{W}_{\mathbf{k}'}(\mathbf{k}) \equiv \begin{pmatrix} W^{11}_{\mathbf{k}',\gamma}(\mathbf{k}) & W^{12}_{\mathbf{k}',\gamma}(\mathbf{k}) \\ W^{21}_{\mathbf{k}',\gamma}(\mathbf{k}) & W^{22}_{\mathbf{k}',\gamma}(\mathbf{k}) \end{pmatrix}. \tag{B4}$$

The elements of $\overleftrightarrow{W}$ are conveniently given in terms of the nearest-neighbor vectors $\mathbf{n}_a$ of the A sites of the diamond lattice,

$$\mathbf{n}_0 = \frac{1}{4}(1,1,1), \quad \mathbf{n}_1 = \frac{1}{4}(1,-1,-1), \tag{B5}$$

$$\mathbf{n}_2 = \frac{1}{4}(-1,1,-1), \quad \mathbf{n}_3 = \frac{1}{4}(-1,-1,1). \tag{B6}$$

Then

$$\begin{aligned} W^{11}_{\mathbf{k}',\gamma}(\mathbf{k}) &= W^{22}_{\mathbf{k}',\gamma}(\mathbf{k}) \\ &= -J_m + J_2\sum_{a\neq b} e^{i\mathbf{k}\cdot(\mathbf{n}_a-\mathbf{n}_b)}\cos\mathbf{k}'\cdot(\mathbf{n}_a-\mathbf{n}_b), \end{aligned} \tag{B7}$$

$$\begin{aligned} W^{12}_{\mathbf{k}',\gamma}(\mathbf{k}) &= [W^{21}_{\mathbf{k}',\gamma}(\mathbf{k})]^* \\ &= J_1\sum_a e^{i\mathbf{k}\cdot\mathbf{n}_a}\cos(\mathbf{k}'\cdot\mathbf{n}_a+\gamma) \\ &\quad + \frac{1}{2}J_3\sum_{a\neq b\neq c\neq a} e^{i\mathbf{k}\cdot(\mathbf{n}_a+\mathbf{n}_b-\mathbf{n}_c)} \\ &\quad \times\cos[\mathbf{k}'\cdot(\mathbf{n}_a+\mathbf{n}_b-\mathbf{n}_c)+\gamma]. \end{aligned} \tag{B8}$$

Here the sums range over distinct values of a, b, and c taken from 0, 1, 2, and 3.

APPENDIX C: FREQUENCY INTEGRALS OF GREEN'S FUNCTIONS AND MOMENTUM INTEGRATION IN BRILLOUIN ZONE

In this appendix, we give some details of the frequency integrals of Green's functions and the transformation to unit variables x_i in momentum space. The frequency integrals of the correlation functions defined in Eq. (79) can be calculated analytically using the following relations:

$$\int_\omega \frac{1}{\omega^4 + p_1\omega^2 + p_2} = \frac{1}{2\sqrt{p_1}\sqrt{p_1 + 2\sqrt{p_2}}},$$

$$\int_\omega \frac{\omega^2}{\omega^4 + p_1\omega^2 + p_2} = \frac{1}{2\sqrt{p_1 + 2\sqrt{p_2}}}.$$

The frequency integrated Green's functions $\overleftrightarrow{G}_{\chi(\xi)}(\mathbf{k})$ can be written as

$$\overleftrightarrow{G}_{\chi(\xi)}(\mathbf{k}) \equiv \begin{pmatrix} G^{11}_{\chi(\xi)}(\mathbf{k}) & G^{12}_{\chi(\xi)}(\mathbf{k}) \\ G^{21}_{\chi(\xi)}(\mathbf{k}) & G^{22}_{\chi(\xi)}(\mathbf{k}) \end{pmatrix}, \tag{C1}$$

with

$$G^{11}_{\chi}(\mathbf{k}) = G^{22}_{\chi}(\mathbf{k}) = \frac{1}{C(\mathbf{k})}[\overleftrightarrow{B}^{11}(\mathbf{k}) + D(\mathbf{k})\overleftrightarrow{A}^{11}(\mathbf{k})], \tag{C2}$$

$$G^{12}_{\chi}(\mathbf{k}) = [G^{21}_{\chi}(\mathbf{k})]^* \tag{C3}$$

$$= \frac{1}{C(\mathbf{k})}[\overleftrightarrow{B}^{12}(\mathbf{k}) - D(\mathbf{k})\overleftrightarrow{A}^{12}(\mathbf{k})]. \tag{C4}$$

Here $\overleftrightarrow{A}^{\alpha}(\mathbf{k})$ is the α matrix element of $\overleftrightarrow{A}(\mathbf{k})$ defined in Eq. (B3). Then, $C(\mathbf{k})$ and $D(\mathbf{k})$ are

$$C(\mathbf{k}) \equiv 2\sqrt{\mathrm{Tr}[\overleftrightarrow{A}(\mathbf{k})\overleftrightarrow{B}(\mathbf{k})] + 2|\overleftrightarrow{A}(\mathbf{k})\overleftrightarrow{B}(\mathbf{k})|},$$

$$D(\mathbf{k}) \equiv \sqrt{\frac{|\overleftrightarrow{B}(\mathbf{k})|}{|\overleftrightarrow{A}(\mathbf{k})|}}.$$

It is natural from Eq. (B1) that $\overleftrightarrow{G}_{\xi}(\mathbf{k})$ can be expressed $\overleftrightarrow{G}_{\chi}(\mathbf{k})$ with the changes $\overleftrightarrow{A}(\mathbf{k}) \leftrightarrow \overleftrightarrow{B}(\mathbf{k})$.

The numerical integration of the momentum in the first Brillouin zone can be easily evaluated using the transformation to the unit variables in momentum space,

$$\mathbf{k} = \mathbf{b}_1 x_1 + \mathbf{b}_2 x_2 + \mathbf{b}_3 x_3,$$

$$\mathbf{b}_i = \frac{2\pi \mathbf{a}_j \times \mathbf{a}_k}{\mathbf{a}_i \cdot (\mathbf{a}_j \times \mathbf{a}_k)},$$

where $\mathbf{a}_i$ are the fcc primitive vectors, permutations of 1/2(0,1,1). Hence we can transform the momentum k to unit variables x_i, then the momentum integration in the first Brillouin zone can be written as

$$v_{\mathrm{uc}} \int_{\mathrm{BZ}} \frac{d^3\mathbf{k}}{(2\pi)^3} \rightarrow \prod_{i=1}^{3} \left[\int_0^1 dx_i \right]. \tag{C5}$$

[1] H. Katsura, N. Nagaosa, and A. V. Balatsky, Phys. Rev. Lett. **95**, 057205 (2005).
[2] A. Ramirez, Annu. Rev. Mater. Sci. **24**, 453 (1994).
[3] N. Tristan, J. Hemberger, A. Krimmel, H. A. Krug von Nidda, V. Tsurkan, and A. Loidl, Phys. Rev. B **72**, 174404 (2005).
[4] T. Suzuki, H. Nagai, M. Nohara, and H. Tagaki, J. Phys.: Condens. Matter **19**, 145265 (2007).
[5] V. Fritsch, J. Hemberger, N. Buttgen, E. W. Scheidt, H. A. Krug von Nidda, A. Loidl, and V. Tsurkan, Phys. Rev. Lett. **92**, 116401 (2004).
[6] D. Bergman, J. Alicea, E. Gull, S. Trebst, and L. Balents, Nat. Phys. **3**, 487 (2007).
[7] A. Krimmel, M. Mucksch, V. Tsurkan, M. M. Koza, H. Mutka, C. Ritter, D. V. Sheptyakov, S. Horn, and A. Loidl, Phys. Rev. B **73**, 014413 (2006).
[8] P. Chaikin and T. Lubensky, *Principles of Condensed Matter Physics* (Cambridge University Press, Cambridge, England, 1995).
[9] L. Savary, S. Trebst, J. Alicea, D. Bergman, and L. Balents (unpublished).
[10] L. Landau and E. Lifshitz, *Electrodynamics of Continuous Media* (Pergamon, New York, 2002).
[11] I. Dzyaloshinskii, Sov. Phys. JETP **10**, 628 (1960).
[12] M. Kenzelmann, A. B. Harris, S. Jonas, C. Broholm, J. Schefer, S. B. Kim, C. L. Zhang, S. W. Cheong, O. P. Vajk, and J. W. Lynn, Phys. Rev. Lett. **95**, 087206 (2005).
[13] M. Mostovoy, Phys. Rev. Lett. **96**, 067601 (2006).
[14] Y. Aharonov and A. Casher, Phys. Rev. Lett. **53**, 319 (1984).